High-aspect-ratio nanoimprinted structures for a multi-pole magnetic scale

Zhi-Hao Xu[1], Chien-Li Wu[1], Cheng-Kuo Sung[1,*], Sheng-Ching Wang[3], Tsung-Shune Chin[2]

[1]*Department of Power Mechanical Engineering, National Tsing Hua University, Hsinchu 30013, TAIWAN*

[2]*Department of Materials Science & Engineering, Feng Chia University, Taichung 40724, TAIWAN*

[3]*Department of Mechanical Engineering, National United University, Miaoli 36003, TAIWAN*

[*]cksung@pme.nthu.edu.tw, +886-3-5742918

Abstract

Conventional non-structured magnetic scales can only achieve a pole pitch of around 1 mm by dedicate magnetization process; a smaller magnetic pole pitch yields a higher resolution. This study describes a practical approach to obtain high resolution multi-pole magnetic scales using high-aspect-ratio nanoimprinted structures. The dimensions of structure were designed according to demagnetization curve of a magnet, which indicates that a high-aspect-ratio structure is required. Simulation results show that the high-aspect-ratio grating has a larger magnetic strength, steeper variation, and greater tolerance of detection gap than those of low-aspect-ratio gratings. Magnetic flux density in the z direction increases significantly with a decrease of the detection gap. High magnetic strength and flux density contrast benefit signal detection and processing. Nanoimprint technology has shown its potential to fabricate a multi-pole magnetic scale with a pole-pitch of down to 72 nm. To further implement we need to optimize magnetic materials and magnetic sensors such as those widely used in T-bit hard disks, CoCrPt media and giant magneto-resistance sensors.

Keywords: Nanoimprint, Pole pitch, Magnetic scale, Demagnetization factor, High-aspect-ratio structures

1 Introduction

Magnetic encoders have been widely used for precision positioning in operations of machine tools. They are the only choice among various encoders in a harsh environment involving dust, oil, and splash fluids. Such encoders basically comprise a magnetic sensing unit and a multi-pole magnetic scale to pinpoint the exact position. These features of a magnetic encoder have been compared with an optical encoder (Miyashita 1987). A smaller magnetic pole pitch yields a higher resolution. Some factors were proposed for multi-pole magnet system of high resolution magnetic encoder (Luo 1993). Conventional non-structured scales can only achieve a pole pitch around 1 mm by dedicate magnetization process. To obtain higher resolution, previous studies suggested several solutions. For example, a linear pulse motor (LPM) mover in a magnetic encoder was designed (Kikuchi 2000). The LPM was made of carbon steel with a tooth structure as a multi-pole magnetic component, which can achieve a 0.8 mm tooth pitch. A printed circuit board was proposed to fabricate a wire-circuit pattern with periodic 1-dimensional structures (Chiu 2005). A magnetic pole pitch of 0.3 mm was achieved by applying a current of 1 A to the components. The purpose of this study is to propose a design aiming at further improve resolution at sub-micron levels. We demonstrate herewith a new solution by preparing a scale with 72-nm-magnetic-pole-pitch using nanoimprint lithography process.

2 Design Principle

To obtain high magnetic flux density for a multi-pole magnetic scale, the aspect ratio of the structure is designed using the demagnetization curve of a typical magnet. Once a magnet scale is

manufactured, a strong field H_1 is applied to magnetize it. Upon removal of the magnetizing field, the induction B will fall following the path shown in Fig. 1. The operating point P of the magnet is determined by the intersection of the load line OC with the second quadrant of the hysteresis loop, known as the demagnetization curve. The load line OC with angle β to the ordinate is determined by the demagnetizing factor N_d, which is shown in Eq. (1).

$$\cot\beta = \left(\frac{4\pi - N_d}{N_d}\right) \quad (1)$$

The N_d depends mainly on the shape of the body and can be calculated exactly only for an ellipsoid (Cullity 1972). The structure of the magnet scale, as shown in Fig. 2, was modeled as an elliptic cylinder with the linewidth b and height c, and then the value of N_d was approximated by using Eq. (2) (Osborn 1945).

$$N_d = \frac{4\pi c}{(b+c)} \quad (2)$$

Having an increased demagnetization factor N_d means that the loading line OC tends to lie at a higher angle β to result in a larger demagnetizing field H_d, which causes a decreased residual magnetic induction B_d. This is quantitatively depicted in Eq. (3). According to the principle of demagnetization factor and direction of magnetization, the high-aspect-ratio structure has a small demagnetizing field H_d. Therefore, its magnetic flux density is higher than that of low-aspect-ratio structure.

$$B_d = -\left(\frac{4\pi - N_d}{N_d}\right) H_d \quad (3)$$

3 Simulation model

Magnetic simulation was employed to attain a half-period single sine/cosine wave of 72 nm from the magnetic structures. The half-period waveform comes from magnetic pole pitch of the magnetic scale. The waveform was obtained from sensed magnetic flux density in z direction, at a detection gap 100 nm above the surface of the structure (Fig. 2). Herein, we employed commercial sofware *Maxwell 15 Ansys* to simulate the magnetic flux density distribution. The balloon boundary condition was used in the model, which was suitable for magnetic leakage. The magnetic scale with a grating linewidth of 72 nm and grating pitch of 144 nm were first designed and simulated using NdFeB magnet as an example. The grating heights were varied with 24 nm, 72 nm, and 200 nm to compare the effect of the aspect ratio. The grating profiles in all models were rectangular. In order to compare with the experimental results, the ideal profile was then modified to the as-fabricated profile in simulation. Finally, the gap was decreased to observe the change in sensed magnetic flux density.

4 Experimental setup

The schematic of the fabrication process for high-aspect-ratio structures is shown in Fig. 3. To obtain a high-aspect-ratio magnetic grating, nanoimprint process is first applied on a glass substrate to define 144-nm-pitch resist gratings without a residual layer; the sample size is 5 cm $\times$ 5 cm. The grating height, linewidth, and pitch of the stamp were 180 nm, 95 nm, and 144 nm, respectively. The resist was spin-coated on a glass substrate with a thickness of 80 nm. By using a plasma trimming technique to obtain thin and high-aspect-ratio resist strucutres, 21-nm-wide resist gratings

were obtained on the substrate. The plasma trimming was conducted using the argon 65 sccm flow rate and oxygen 2.5 sccm in an anisotropic etching mode by a reactive-ion etching (RIE) machine (PC-300, SAMCO Inc.); the RF power was 250 W and the operating pressure was 28 Pa (Lin 2012). Thereafter, a magnetic material such as NdFeB was thermally evaporated onto one side of the grating with an oblique deposition angle 35° (Wu 2013). Aluminum with a coating thickness of 60 nm is demonstrated as a substitute for NdFeB for the feasibility study. NdFeB will interfere with the electron beam during the inspection with Scanning Electron Microscope (SEM) leading to worse SEM images at high magnifications. Then, the resist material is removed by plasma etching. To prevent the metallic structure from oxidation, especially for oxygen-sensitive materials e.g. NdFeB, argon plasma can be used as the primary operation gas. The final component is totally inorganic, which exhibits excellent thermal resistance and mechanical strength.

5 Results and discussion

After applying nanoimprint processing to define a grating width of 72 nm, a single direction and high magnetic field was then employed to magnetize the gratings. Fig. 4 shows the direction of magnetic flux density after magnetization using a magnetic grating pitch of 144 nm, linewidth of 72 nm, and height of 200 nm. The magnetization process employed in this study is much simpler than the conventional magnetization process for magnetic scale (Luo 1993). Conventional magnetization process requires a precision machining process and complicate magnetization platform involving a high-precision positioning stage, magnetizing head, and specified magnetizing current (Luo 1993).

Fig. 5 shows the magnetic flux density simulated with varying structure heights (24 nm, 72 nm, and 200 nm) and a fixed grating pitch of 144 nm, linewidth of 72 nm, and gap of 100 nm. It indicates that high-aspect-ratio grating has high magnetic flux density and peak-to-peak value in z direction. The simulation results also show that the demagnetization field of the high-aspect-ratio structure is smaller than that of low-aspect-ratio structure. Based on the aforementioned design principle, the demagnetization factors of 9.42, 6.28, and 3.33 were calculated from Eq. (2) with grating heights of 24 nm, 72 nm, and 200 nm, respectively; the loading lines have angles β of 71.56, 45, and 19.8 degrees, respectively. The calculated results show the high-aspect-ratio structure with high residual induction magnetic flux density. The half period single sine/cosine waves of 72 nm were obtained from the magnetic structures. These are crucial for processing the signal to obtain a resolution better than 72 nm. For example, the signal can be interpolated by 10 folds, which results in the resolution of 7.2 nm. The magnetic flux density in z direction of the as-fabricated grating profile is shown in Fig. 5, which indicates the waveform and magnitude are conformal with ideal rectangular grating profile. This demonstrates that the fabrication approach is suitable for this application.

The detection gap of 100 nm was applied to produce the simulation results shown in Fig. 5. The detection gap is generally smaller than a pole pitch in commercial encoders, because a smaller gap generates higher signal strength. Similarly, the detection gap was chosen to be 300 um above the pole pitch of 350 um (Chiu 2005).The magnetic flux density in z direction increases significantly with a decrease of the detection gap, as shown in Fig. 6. It is also meaningful to the signal detection and processing. However, it would be challenging to achieve a detection gap of less than 100 nm

constantly for a long measuring distance. As the detection gap was 100 nm, the peak-to-peak magnetic flux densities in z direction were simulated to be 93.9 Gs, 89.7 Gs, and 63.2 Gs with respect to aspect ratios of 2.78, 1, and 0.33, respectively. With the same approach, the least detection gaps for the aspect ratios of 2.78, 1, and 0.33, were computed to be 120 nm, 116nm and 110 nm, respectively.

Figure 7 shows the imprinted 144-nm-pitch resist gratings without a residual layer with a linewidth of 50 nm and a height of 180 nm. The resist structure has a height of 128 nm, linewidth 21 nm, and grating pitch 144 nm after anisotropic plasma trimming process (shown in Fig. 8a). The trimming was not isotropic reduction in both width and height. The structure height reduction is much higher than the linewidth reduction. To obtain the SEM images at high magnifications, aluminum was demonstrated as a substitute for magnetic material. The resist material was removed by plasma etching, which can be observed in Fig. 8b; the profile of metallic grating was not significantly influenced by the resist profile after resist removal. This is contributed by the ultra-fine and high-aspect-ratio grating profiles. The final structured magnetic components are inorganic thus are stable and strong. According to these results, nanoimprint lithography has the potential to push to an ultimate resolution for magnetic encoders as the new paradigm. However, it requires further implementation in magnetic materials and magnetic sensors. A CoCrPt thin film has been widely used in T-bit hard disks and studied in many papers; but, few papers for hard magnetic structures. It is the first choice to optimize magnetic material, CoCrPt, for further implementation. For magnetizing sensors, the smallest active area (10 um^2) of the existing hall probe is bigger than the

linewidth of 72 nm. In addition, the smallest commercially available magneto-resistance sensors can only detect a single half-period signal of 120 um. According to these reasons, to further implement we need to optimize magnetic materials and magnetic sensors such as CoCrPt and giant magneto-resistance sensors.

6 Conclusions

Nanoimprint lithography has demonstrated its potential to fabricate high resolution magnetic scales with a pole pitch down to 72 nm. Simulation results indicate that using high-aspect-ratio magnetic gratings, the waveform and magnetic flux density are greatly improved. Consequently, a resolution enhancement is achieved by a factor of 13889x (1 mm / 72 nm) using the proposed solution, and meanwhile, the ultra-small detection gap is no longer required for obtaining sufficient signal strength. The fabrication approach can be further extended to continuous roll-to-roll processing for a long magnetic stripe. To further implement we need to optimize magnetic materials and magnetic sensors such as those widely used in T-bit hard disks, CoCrPt media and giant magneto-resistance sensors.

References

B. D. Cullity (1972) Introduction to magnetic materials. Notre Dame, Indiana.

C. H. Lin, C. L. Wu, and C. K. Sung (2012) Tunable-linewidth nanoimprint working stamps fabricated by double oblique metal deposition. Technical Proceedings of the NSTI-Nanotech (Santa Clara) 2 (Florida: Taylor & Francis), 512-515.

C. L. Wu, C. K. Sung, P. H. Yao, and C. H. Chen (2013) Sub-15 nm linewidth gratings using roll-to-roll nanoimprinting and plasma trimming to fabricate flexible wire-grid polarizers with

low colour shift. Nanotechnology 24 265301 (7pp).

J. A. Osborn (1945) Demagnetizing factors of the general ellipsoid. PHYSICAL REVIEW, Vol. 67, 351-357

K. C. Chiu, D. R. Huang, H. P. Shieh (2005) Formulas for computing the magnetic flux density of fine magnetic pole pitch fabricated on printed circuit board. Journal of Magnetism and Magnetic Materials 290–291, 1304-1308.

K. Miyashita, T. Takahashi, M. Yamanaka (1987) Features of a magnetic rotary encoder. IEEE Trans. Magn. 23, 2182-2184.

Y. Kikuchi, T. Yoneda, Y. Kataoka, K. Shiotani, H. Wakiwaka, H. Yamada (2000) Considerations of output voltage waveform on magnetic linear encoder for artificial heart using linear pulse motor. Sens. Actuator A-Phys. 81, 309-312.

Y. J. Luo, E. T. Hwang, S. M. Huang (1993) Multi-pole magnetization of high resolution magnetic encoder. Proceedings, EEIC/ICWA Exposition, Chicago, USA, Oct. 4-7, 237-242.

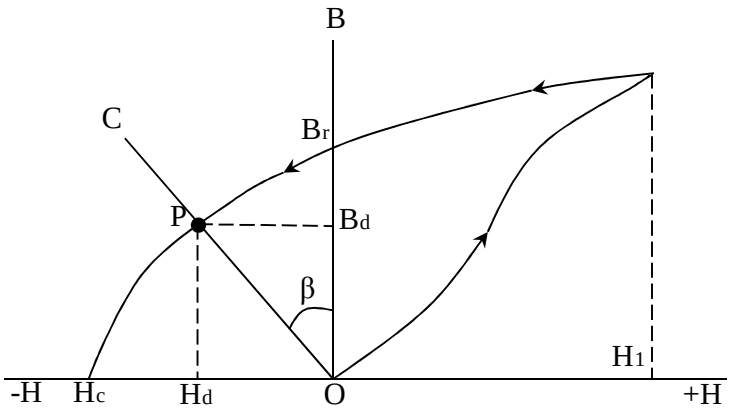

Fig. 1 Demagnetizing induction B_d in an open magnetic circuit

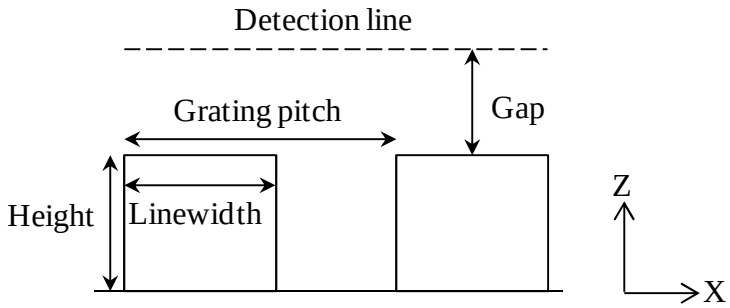

Fig. 2 Simulation model

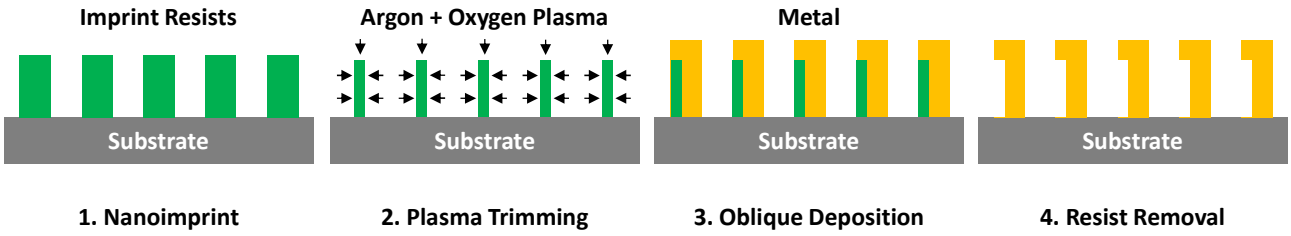

Fig. 3 Schematic of fabrication process for fine-pitch magnetic gratings

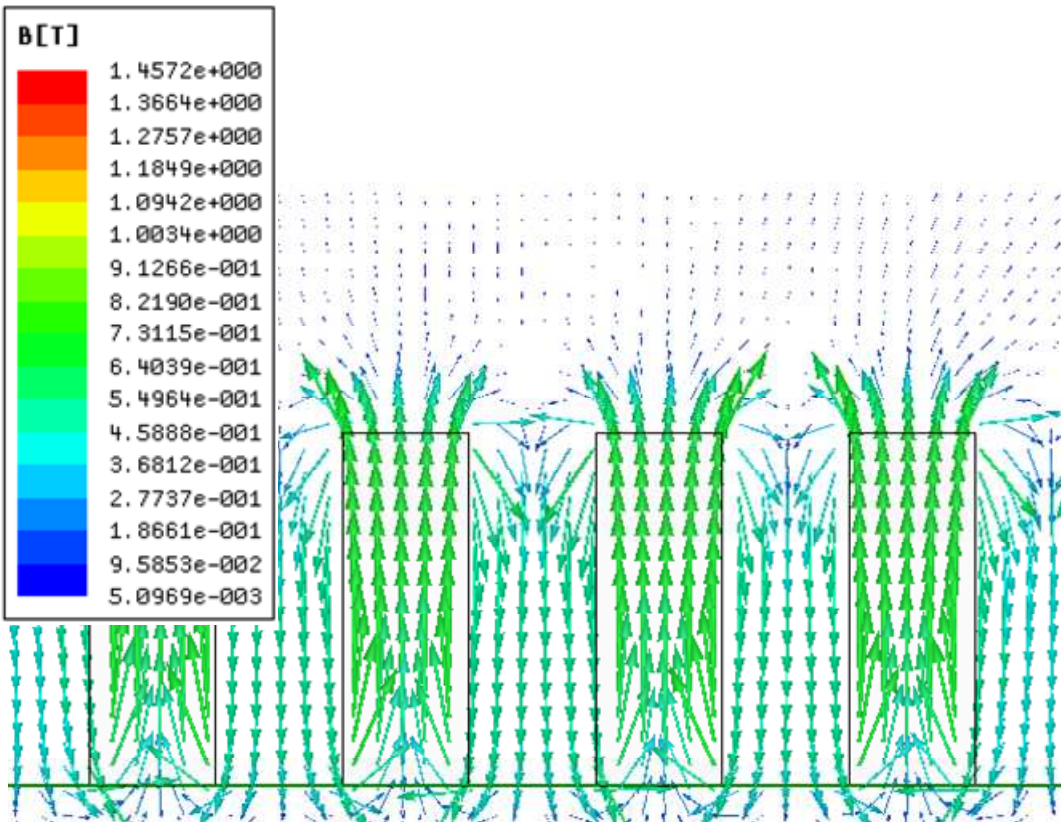

Fig. 4 Simulation results of the magnetic flux density distribution with a grating linewidth of 72 nm and height of 200 nm

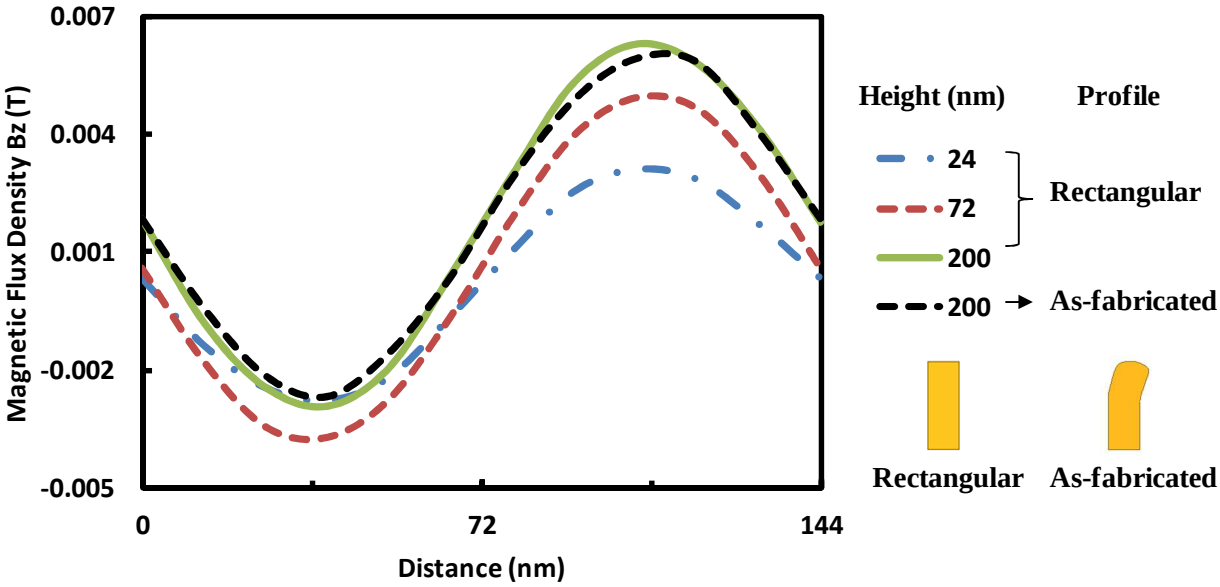

Fig. 5 Simulations results of the magnetic flux density with various structure heights with linewidth 72 nm and gap 100 nm

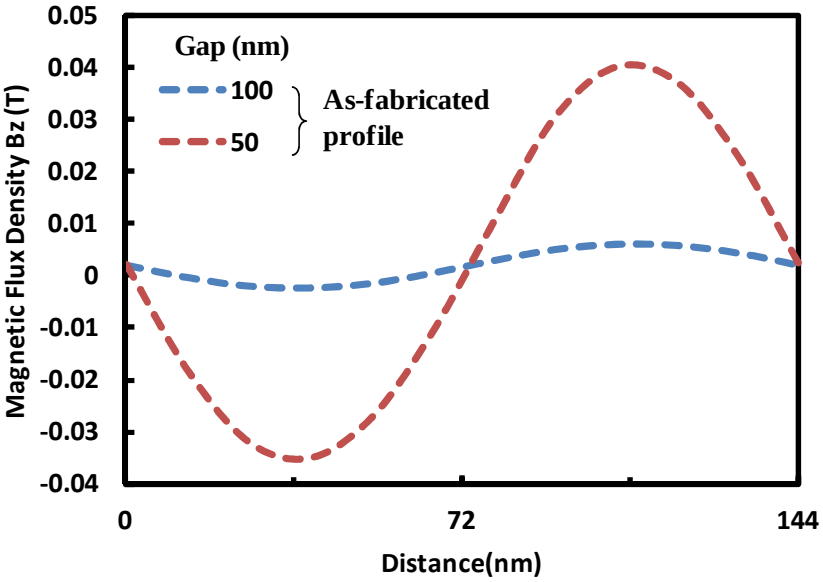

Fig. 6 Simulation results of the magnetic flux density with two detection gaps with linewidth 72 nm and height 200 nm

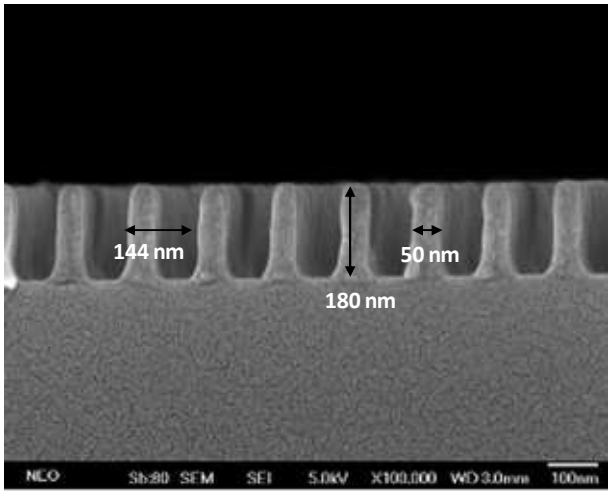

Fig. 7 SEM image of imprinted resist gratings without a residual layer with a linewidth of 50 nm and a height of 180 nm

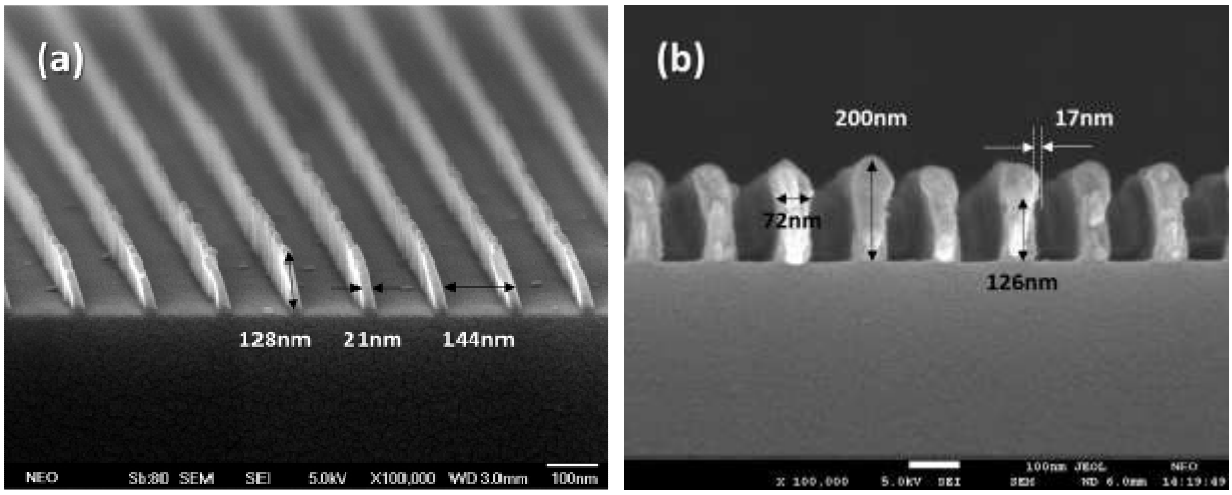

Fig. 8 SEM images of (a) resist gratings with a linewidth of 21 nm after plasma trimming process, and (b) the final metallic/aluminum gratings which are pure inorganic after removing the resist material